



Complementary consistency semi-supervised learning for 3D left atrial image segmentation

Hejun Huang^a, Zuguo Chen^{a,b,*}, Chaoyang Chen^a, Ming Lu^a, Ying Zou^a

^aSchool of Information and Electrical Engineering, Hunan University of Science and Technology, Xiangtan 411201, China

^bShenzhen Institute of Advanced Technology, Chinese Academy of Sciences, Shenzhen 518055, China

ARTICLE INFO

Article history:

Keywords: Complementary consistency, Semi-supervised segmentation, Complementary auxiliary models, Uncertainty

ABSTRACT

A network (CC-Net) based on complementary consistency training is proposed for semi-supervised left atrial image segmentation in this paper. From the perspective of complementary information, CC-Net efficiently utilizes unlabeled data and resolves the problem that semi-supervised segmentation algorithms currently in use have limited capacity to extract information from unlabeled data. A primary model and two complementary auxiliary models are part of the complementary symmetric structure of the CC-Net. The inter-model perturbation is formed between the main model and the auxiliary model to form complementary consistency training. The complementary information between the two auxiliary models helps the main model to focus on the fuzzy region effectively. Additionally, forcing consistency between the main model and the auxiliary models makes it easier to obtain decision boundaries with low uncertainty. CC-Net was validated in the benchmark dataset of the 2018 Atrial Segmentation Challenge. The Dice reached of 89.82% with 10% labeled data training and 91.27% with 20% labeled data training. By comparing with current state-of-the-art algorithms, CC-Net has the best segmentation performance and robustness. Our code is publicly available at <https://github.com/Cuthbert-Huang/CC-Net>.

© 2022 Elsevier B. V. All rights reserved.

1. Introduction

Atrial fibrillation (AF) is the most common heart rate disorder, which more significantly affects global mortality and is one of the major burdens of the global healthcare system (Guglielmo et al., 2019). The structure of the left atrium (LA) is essential information for clinicians to diagnose and treat AF (Ikenouchi et al., 2021). The study and treatment of AF rely on proper segmentation of the left atrium. The traditional method of manual segmentation, which is empirically dependent and error-prone, has many drawbacks (Xiong et al., 2021). Au-

tomatic segmentation of the left atrium has been achieved using deep learning-based methods. Chen et al. (2019) obtained accurate segmentation by constructing a multi-task learning framework with shared features among tasks. Li et al. (2019) proposed the attention-based hierarchical aggregation network (HAANet), which makes better use of the attention mechanism to improve the ability of effective feature extraction and hierarchical aggregation to improve the ability of network feature fusion. The supervised learning methods described above show good segmentation performance, but they rely on a large amount of labeled data for training. Due to the difficulty and high expense of annotation, there are few 3D medical image annotation datasets. Therefore, the critical issue is how to get acceptable segmentation performance with less annotated data.

*Corresponding author.
e-mail: zg.chen@hnust.edu.cn (Zuguo Chen)

Semi-supervised learning refers to a method that uses a large amount of unlabeled data to learn with a small amount of labeled data. This method is better applicable to scenes where labeled data is difficult to obtain (van Engelen and Hoos, 2020). Semi-supervised learning is particularly efficient in 3D left atrial segmentation. Based on the mean teacher model, Yu et al. (2019) employed uncertainty maps to direct the student model to gradually gain trustworthy information from the teacher model and obtained good left atrium segmentation results. Signed-distance map regression was utilized by Li et al. (2020) to add shape and location prior information while discriminators were used as regularization terms to improve segmentation stability. Recognizing the perturbations between the regression and prediction tasks, Luo et al. (2021) built a dual-task consistency loss to learn unlabeled data during inter-task transitions, improving the generalization of the model. All of the aforementioned efforts successfully segmented the left atrium, but they were unable to uncover information about the challenging area of unlabeled data. To produce low-entropy predictions of uncertainty regions, MC-Net+ (Wu et al., 2022) builds mutual consistency amongst decoders using three alternative upsampling techniques and obtains successful results. However, there is only conservative learnable information exists across probability maps produced by various upsampling techniques, and the learnable information weakens over time due to the common encoder, which prevents MC-Net+ from correctly segmenting data in the key uncertainty region (see the qualitative analysis subsection 4.3 for a comparison of our method with MC-Net+).

We define accurate segmentation as a process that combines high-level semantic information with high-resolution detail information. By paying more attention to high-level semantic information, the deterministic segmentation region’s boundary can be broadened, which lowers the false negative rate. An increase in the true positive rate results from paying more attention to high-resolution detail data, which entails lowering the uncertainty of the right segmentation boundary. Can the model be modified to concentrate more on high-level semantic information or more on high-resolution detail information to obtain probability maps with rich learnable information? The skip-connection is crucial to V-Net (Milletari et al., 2016) and aids in recovering high-resolution detail data that was lost during upsampling due to encoding. By altering the V-Net decoder’s layer’s use of skip-connection, Complementary A and Complementary B can be produced. After training with 10% labeled data, Complementary A, Complementary B, and V-Net segmentation results are compared in Fig. 1. Complementary A shifts its emphasis away from high-rate detail information and toward high-level semantic information. Complementary A has a wider segmentation boundary in the challenging branch section (the arrow part of the figure), as shown in the second line of Fig. 1(c). The Complementary A segmentation region essentially wraps the true label, as shown by the third row of Fig. 1(c). A portion of the high-level semantic information is dropped in Complementary B in favor of a greater emphasis on high-rate detail information. The challenging branching part of Complementary B has more believable segmentation bound-

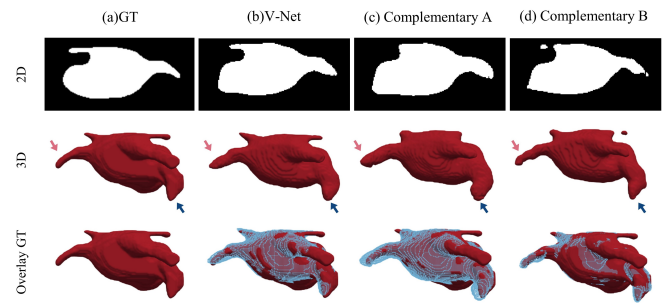


Fig. 1. Comparison of segmentation results of Complementary A, Complementary B, and V-Net after training with 10% labeled data, where Complementary A is obtained from the second and fourth layers of the V-Net decoder without skip-connection, and Complementary B is obtained from the first and third layers of the V-Net decoder without skip-connection.

aries, as shown in the second line of Fig. 1(d). The third line of Fig. 1(d) demonstrates how the true labels essentially encircle the Complementary B segmentation region. The aforementioned findings suggest that the probability maps produced by the Complementary A and Complementary B models contain a wealth of learnable information.

Therefore, this paper takes the V-Net as the primary model, constructs two complementary auxiliary models simultaneously, and proposes a new network based on complementary consistency training. The two auxiliary models form a complementary symmetric structure by varying whether a layer of the V-Net decoder uses skip-connection or not. The probability maps produced by the two auxiliary models, which contain a wealth of learnable information, are transformed into pseudo-labels in this paper using a sharpening function to improve the training of the main model. This process draws on cross-pseudo-supervision (Chen et al., 2021) and mutual consistency (Wu et al., 2021). The main model’s high-quality probability maps are also converted into pseudo-labels to direct the auxiliary model’s training. Complementary consistent training is created by inter-model perturbation between the primary model and the auxiliary model. Dice loss is employed as a supervised loss for labeled input data. The regularity loss of the inter-model consistency is used as the unsupervised loss for all input data. Only the primary model is used for testing after training, greatly reducing the network parameters during testing while still achieving precise segmentation results. In this paper, the effectiveness of the proposed method is verified on the dataset of the left atrial segmentation challenge in 2018, and we find that it can produce results that are on par with V-Net training on 100% labeled data using only 20% labeled data and 80% unlabeled data. When compared to other cutting-edge techniques, our method currently offers the best segmentation results. Consequently, the contributions and novelty of this paper are summarised as follows:

- A semi-supervised learning method based on complementary consistency training is proposed in this paper. The method makes full use of unlabeled data from the perspective of complementary information.

- The construction method for complementary symmetric structures that produce rich complementary learnable information is developed in this paper.
- The proposed method in this paper was validated on the dataset of the 2018 Atrial Segmentation Challenge. The results show that the method greatly enhances the utilization of unlabeled data, with excellent segmentation performance and robustness.

2. Related work

2.1. Semi-supervised segmentation

Semi-supervised segmentation has undergone extensive development intending to extract as much useful information as possible from unlabeled data due to the high cost and difficult-to-obtain properties of labeled data in segmentation tasks. For generative adversarial learning, Zhai *et al.* (2022) defines two asymmetric generators and a discriminator. The discriminator filters the masks produced by the generators to provide supervised information that enables the network to learn from unlabeled data. To help the student model learn more information, Xiao *et al.* (2022) added a teacher model that combines CNN and Transformer structures to the mean teacher model. Zhang *et al.* (2022) suggested a double error correction method to improve the quality of pseudo tags and improve segmentation performance. In this paper, we build two complementary auxiliary models to aid the main model in exploring the ambiguous areas of unlabeled data, while the complementary consistency between the main model and the auxiliary model effectively learns from unlabeled data.

2.2. Consistency regularization

Consistent regularization is a common and effective method in semi-supervised learning. Luo *et al.* (2021) introduced a dual-task consistency between the directly predicted segmented map and the level set-derived segmented map taking into account the inherent perturbations between the related tasks. Liu *et al.* (2022) expands the segmentation model by including a classification model. The classification model produces the output prediction graph's class vector, which is then used to construct the contrast consistency loss. Wang *et al.* (2022a) created a bi-consistent segmentation network by combining the model-level perturbation with the input spatial contextual perturbation. Hu *et al.* (2022) created attention-guided consistency by integrating self-attention into the mean teacher model and encouraging model attention maps to be consistent at the feature level. Chen *et al.* (2022b) used the cross-modal coherence of unpaired CT and MRI to learn modality-independent information in the cross-modal domain. Ouali *et al.* (2020) suggested using cross-consistency to compel primary and secondary decoders to choose low-density regions. Zhong *et al.* (2021) suggested pixel contrast consistency based on the label consistency property and the inter-pixel feature space contrast property for the perturbation between image enhancement degrees. Our method, which draws its inspiration from mutual consistency, makes use of complementary consistency based on

model consistency to let the primary model learn complementary information from the auxiliary models.

2.3. Multi-view training

The purpose of multi-view training is to improve the learning effect by using the redundant information between perspectives (Yan *et al.*, 2021). Dong-DongChen and WeiGao (2018) constructs three divergent models to generate pseudo-labels with a voting mechanism. The method is ineffective when there is not enough unlabeled data because noise is simultaneously introduced. Using the uncertainty estimates from each view, Xia *et al.* (2020) rotated the input for multi-view collaborative training to produce an accurate segmentation. The method is simple to implement, but it involves more redundant learning and a greater variety of perspectives to achieve more desirable performance. Zheng *et al.* (2022) divided the labeled data into complementary subsets and input to the two training models for training, enhancing the network's capability to explore ambiguous regions. Our method creates two auxiliary models that work in tandem to direct the main model to concentrate on the ambiguous region from two complementary perspectives, while also gaining the advantages of multiple perspectives, to obtain low entropy predictions.

2.4. Uncertainty estimation

Uncertainty estimation is crucial for extracting trustworthy information from unlabeled data and for lowering the randomness of predictions (Chen *et al.*, 2022a). Yu *et al.* (2019) obtained uncertainty maps from the teacher model using Monte Carlo dropout, guiding the student model to gradually obtain reliable information. To learn high-confidence information, Zheng *et al.* (2022) used uncertainty maps as weights for losses. Wu *et al.* (2022) constructed three decoders with different up-sampling methods and used mutual learning methods to obtain low-uncertainty predictions. Wang *et al.* (2022b) employed a triple uncertainty-oriented framework that enabled the student model's three tasks to learn more reliable knowledge from the teacher model. Through mutual learning between the complementary auxiliary model and the main model, our method reduces the uncertainty in the complementary information.

3. Materials and Methods

3.1. Dataset and pre-processing

The method proposed in the paper was evaluated using the benchmark dataset from the 2018 Atrial Segmentation Challenge (Xiong *et al.*, 2021). The dataset includes 154 3D LGE-MRIs that were independently acquired and came from 60 patients with known AF. The spatial resolution of a 3D LGE-MRI scan is $0.625 \times 0.625 \times 0.625$ mm³, with a spatial dimension of $576 \times 576 \times 88$ or $640 \times 640 \times 88$ pixels. Segmentation labels were obtained by manual segmentation by three trained observers in unison, and both the original image and the segmentation labels were stored in NRRD format. The setup of Yu *et al.* (2019); Li *et al.* (2020); Luo *et al.* (2021); Wu *et al.* (2022) is followed in this paper, where 100 images were divided into 80 for training and 20 for testing, with the same preprocessing, due to the limited number of labeled images available (100).

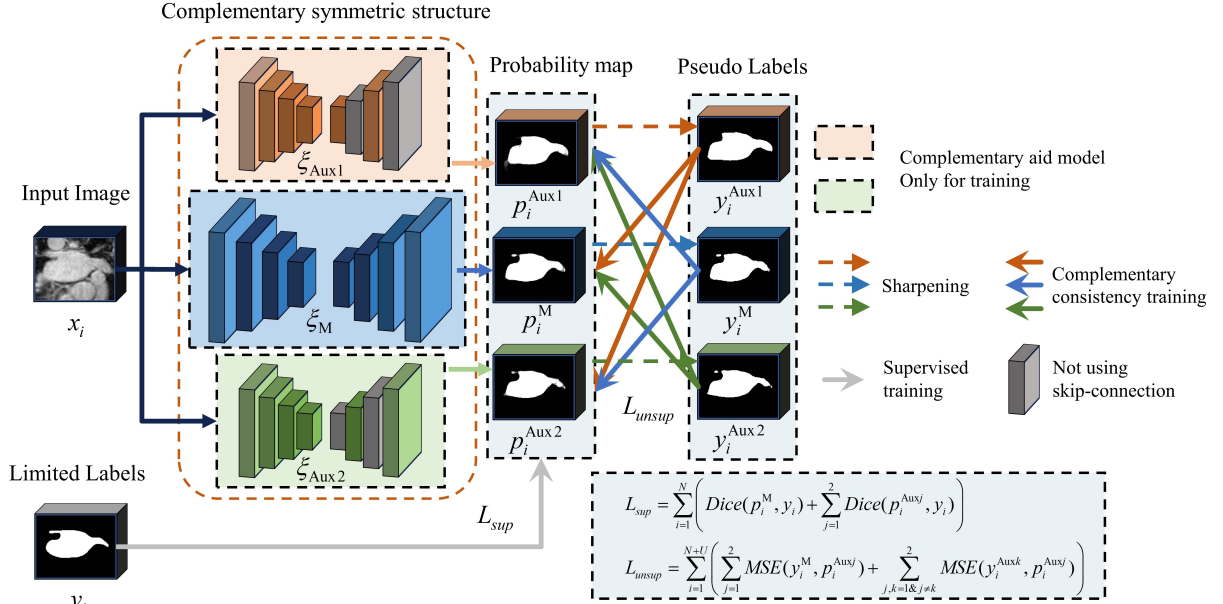


Fig. 2. Overall architecture of CC-Net.

3.2. Network overall architecture

Figure 2 depicts the method's overall architecture in this article. It contains two auxiliary models and one main model. V-Net (Milletari *et al.*, 2016) is used in the main model. The encoders of the two auxiliary models are aligned with the main model, and the decoders form a complementary symmetric structure by cross-spacing using skip-connection. Specifically, the auxiliary model 1 decoder layers 2 and 4 and the auxiliary model 2 decoder layers 1 and 3 do not employ skip-connections. A 3D medical image is the input for the segmentation network. The main and auxiliary models are supervised and trained using real labels if the input is labeled data. If the input is unlabeled data, the two auxiliary models use a complementary symmetric structure to learn complementary information about the same input. This allows them to use the unlabeled data effectively. The sharpening function is used to generate pseudo-labels for the probability maps of the main and auxiliary model outputs. The complementary information learned by one of the auxiliary models is passed through pseudo labels to guide the training of the main model and the other auxiliary model. Meanwhile, the pseudo labels generated by the main model guide both auxiliary models for training. In this way, a complementary consistency training network (CC-Net) with one main model and two complementary auxiliary models is constructed. It is important to note that only the main model is used for reasoning during the inference process and the two auxiliary models are for training, which significantly increases the efficiency. The complementary symmetry structure and complementary consistency training are thoroughly explained in the next two subsections.

3.3. Complementary symmetric structure

Inspired by Wang *et al.* (2022b), the method in this paper learns complementary information by constructing two complementary auxiliary models to efficiently utilize unlabeled data.

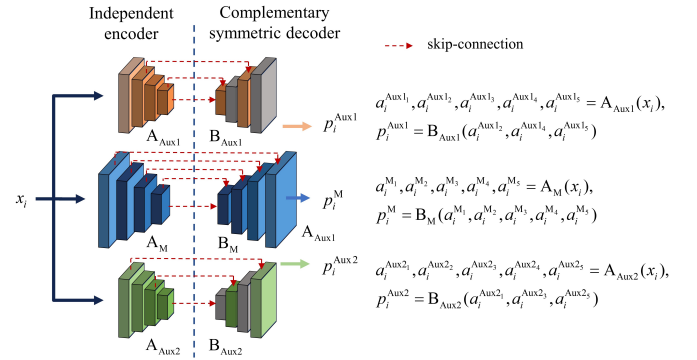


Fig. 3. Specific structure of the complementary auxiliary model.

Fig. 3 illustrates how the main model and the auxiliary model each use separate encoders. Three encoders, designated as A_M , A_{Aux1} , and A_{Aux2} , respectively, all share the same structure. For input x_i , each encoder has 4 coding blocks, all of which produce 5 outputs after 5 convolutions and 4 downsamplings:

$$\begin{aligned} a_i^{Aux1_1}, a_i^{Aux1_2}, a_i^{Aux1_3}, a_i^{Aux1_4}, a_i^{Aux1_5} &= A_{Aux1}(x_i), \\ a_i^{M_1}, a_i^{M_2}, a_i^{M_3}, a_i^{M_4}, a_i^{M_5} &= A_M(x_i), \\ a_i^{Aux2_1}, a_i^{Aux2_2}, a_i^{Aux2_3}, a_i^{Aux2_4}, a_i^{Aux2_5} &= A_{Aux2}(x_i) \end{aligned} \quad (1)$$

where $a_i^{Aux1_j}$ represents the j -th ($0 < j \leq 5$) result produced by the i -th data input to the first auxiliary model encoder, $a_i^{M_j}$ represents the j -th ($0 < j \leq 5$) result produced by the i -th data input to the main model encoder, and $a_i^{Aux2_j}$ represents the j -th ($0 < j \leq 5$) result produced by the i -th data input to the second auxiliary model encoder.

The decoders of the auxiliary model adopt a complementary symmetric structure, with B_M , B_{Aux1} , and B_{Aux2} representing

the decoders of the main model and the two auxiliary models, respectively. Decoder layers 2 and 4 of auxiliary model 1 do not use skip-connection, and the inputs to decoder B_{Aux1} are the final output a_i^{Aux15} and intermediate outputs a_i^{Aux12} and a_i^{Aux14} of encoder A_{Aux1} . Thus the probability map of the auxiliary model 1 is as follows.

$$p_i^{Aux1} = B_{Aux1}(a_i^{Aux12}, a_i^{Aux14}, a_i^{Aux15}) \quad (2)$$

Auxiliary model 1 abandons partial high-resolution feature fusion and focuses more on high-level semantic information. False Negative is reduced by expanding the boundaries of segmentation to include more voxels that should be segmented. Decoder layers 1 and 3 of auxiliary model 2 do not use skip-connection, and the inputs to decoder B_{Aux2} are the final output a_i^{Aux25} and intermediate outputs a_i^{Aux21} and a_i^{Aux23} of encoder A_{Aux2} . Thus the probability map of the auxiliary model 2 is as follows.

$$p_i^{Aux2} = B_{Aux2}(a_i^{Aux21}, a_i^{Aux23}, a_i^{Aux25}) \quad (3)$$

Auxiliary model 2 drops some of the low-resolution feature fusion and focuses more on high-resolution pixel information. True Positive is increased by optimizing the boundaries of segmentation which also reduces the incorrectly segmented voxels. The main model uses the full V-Net, with all four decoding blocks using skip-connection. In this way, it forms a simple inter-model perturbation with the auxiliary model. The probability map of the main model is as follows.

$$p_i^M = B_M(a_i^{M1}, a_i^{M2}, a_i^{M3}, a_i^{M4}, a_i^{M5}) \quad (4)$$

Auxiliary model 1 focuses more on high-level semantic information, while auxiliary model 2 focuses more on high-resolution pixel information. The complementary symmetric structure is formed by a straightforward setup that causes the two auxiliary models to tend in opposing directions while maintaining the compatibility information. This paper uses a straightforward complementary symmetric skip-connection for the complementary symmetry setup. The main model is guided effectively because the two auxiliary models both acquire useful complementary information and create only minor inter-model perturbations.

3.4. Complementary consistency training

If the training set used in this study has N labeled data and U unlabeled data, and if $N \ll U$, then the labeled data set is denoted as $D_L = \{x_i, y_i\}_{i=1}^N$ and the unlabeled data set is $D_U = \{x_i\}_{i=N+1}^{N+U}$, where $x_i \in \mathbb{R}^{H \times W \times D}$ is the input image and $y_i \in \mathbb{R}^{H \times W \times D}$ is the corresponding label. We construct two auxiliary models ξ_{Aux1} and ξ_{Aux2} for the main model ξ_M . The input image x is input to both the main and auxiliary models, and the respective probability maps p_i^M , p_i^{Aux1} and p_i^{Aux2} are obtained from eqs. (1) to (4). The probability map p_i^{Aux1} of the output of ξ_{Aux1} complements the probability map p_i^{Aux2} of the output of ξ_{Aux2} because the two auxiliary models employ complementary symmetric structures. The primary and secondary model probability maps are processed by the sharpening function to obtain

the respective pseudo labels.

$$\begin{aligned} y_i^M &= \text{sharpening}(p_i^M), \\ y_i^{Aux1} &= \text{sharpening}(p_i^{Aux1}), \\ y_i^{Aux2} &= \text{sharpening}(p_i^{Aux2}) \end{aligned} \quad (5)$$

where, $\text{sharpening}()$ represents the sharpening function and is consistent with (Wu *et al.*, 2021).

For the labeled input image $x_i \in D_L$, we use the label $y_i \in D_L$ to guide the learning of the main and auxiliary models. The supervised loss uses the common dice loss. Supervised losses are defined as:

$$L_{sup} = \sum_{i=1}^N \left(\text{Dice}(p_i^M, y_i) + \sum_{j=1}^2 \text{Dice}(p_i^{Auxj}, y_i) \right) \quad (6)$$

where, p_i^M denotes the probability map generated by the primary model for the i -th input, p_i^{Auxj} denotes the probability map generated by the j -th auxiliary model for the i -th input, and Dice represents the dice loss. For all input images, the complementary auxiliary model generates probability maps with rich learnable information, and the pseudo-labels of the complementary auxiliary model guide the training of the main model. Due to the lack of overall segmentation capability of a single auxiliary model, training needs to be guided by the pseudo label generated by the main model and another auxiliary model. The unsupervised loss uses the mean square error (MSE) between the pseudo label and the probability map. Unsupervised loss is defined as:

$$L_{unsup} = \sum_{i=1}^{N+U} \left(\sum_{j=1}^2 \text{MSE}(y_i^M, p_i^{Auxj}) + \sum_{j,k=1 \ \& \ j \neq k}^2 \text{MSE}(y_i^{Auxk}, p_i^{Auxj}) \right) \quad (7)$$

where y_i^M denotes the pseudo label generated by the main model for the i -th input, p_i^{Auxj} denotes the probability map generated by the j -th auxiliary model for the i -th input, y_i^{Auxk} denotes the pseudo label generated by the k -th auxiliary model for the i -th input, and MSE denotes the mean square error. The final loss is the sum of the supervised loss and the unsupervised loss. Therefore, the final loss is defined as:

$$L_{total} = \lambda_s L_{sup} + \lambda_u L_{unsup} \quad (8)$$

where λ_s is the weight coefficient of supervised loss, λ_u is the weight coefficient of unsupervised loss, L_{sup} is used for labeling input images only, and L_{unsup} is used for all input images. According to (Yu *et al.*, 2019; Luo *et al.*, 2021), λ_u use a time-independent Gaussian warming-up function. According to ablation study (subsection 4.5), λ_s is set to 0.3 to enhance the effect of complementary consistency training. The semi-supervised learning algorithm based on complementary consistency training is shown in Algorithm 1.

4. Experiments and results

4.1. Implementing details and evaluation indicators

In this paper, we run tests on a single NVIDIA Tesla V100 in an environment with Pytorch 1.9.1+cuda11.1 and Python 3.6.5.

Algorithm 1 Complementary consistency-based semi-supervised learning,

Input: $x_i \in D_L + D_U, y_i \in D_L$

Output: main model parameters θ

- 1: Initialize iteration = 0, max_iteration = 10000
- 2: $\xi_M(x)$ = main model with parameters θ
- 3: $\xi_{Aux1}(x)$ = auxiliary model 1 with parameters θ_1
- 4: $\xi_{Aux2}(x)$ = auxiliary model 2 with parameters θ_2
- 5: **while** iteration < max_iteration **do**
- 6: Calculate the probability maps p_i^M , p_i^{Aux1} , and p_i^{Aux2} of the primary and secondary models according to eqs. (1) to (4).
- 7: **if** $x_i \in D_L$ **then**
- 8: Calculate the supervised loss L_{sup} according to equation (6).
- 9: **end if**
- 10: Calculate the respective pseudo labels y_i^M , y_i^{Aux1} , and y_i^{Aux2} of the primary and secondary models according to equation (5).
- 11: Calculate the unsupervised loss L_{unsup} according to equation (7).
- 12: Calculate the final loss L_{total} according to equation (8).
- 13: Calculate the gradient of the loss function L_{total} and update the main model parameters θ and auxiliary model parameters θ_1 and θ_2 , by backpropagation.
- 14: iteration = iteration + 1
- 15: **end while**
- 16: **return** θ

We randomly crop the image into blocks of $112 \times 112 \times 80$ for training, and as data enhancement, we randomly rotate and flip the image. We use the SGD optimizer with a learning rate of 0.01 and decaying weights to train 10K iterations. According to Wu et al. (2022), a sharpening function with a temperature constant $T = 0.1$ is used to generate the pseudo labels. All experiments were performed under a random number seed of 1337. In the test, the image is cropped into blocks with steps of 18 in the x and y directions and 4 in the z-direction, and the final result is a recombination of the predicted results of each block. The two auxiliary models are not involved in the testing and the test results are only the output of the master model. All experiments were tested without any post-processing. According to Yu et al. (2019), we chose Dice and Jaccard to assess the interior of the segmentation, and the average surface distance (ASD) and 95% Hausdorff distance (95HD) to assess the edges of the segmentation. The primary evaluation metrics are Dice and Jaccard.

4.2. Quantitative comparisons

Our method is validated on 10% and 20% labels and compared with a variety of excellent algorithms, including the uncertainty-aware mean teacher (UA-MT) (Yu et al., 2019), shape-aware semi-supervised net (SASSnet) (Li et al., 2020), dual-task consistency (DTC) (Luo et al., 2021), mutual consistency network (MC-Net (Wu et al., 2021) and MC-Net+ (Wu et al., 2022)).

Table 1 provides a comparison of the results of using 10% and 20% of the labeled data for training while citing the fully supervised training results of V-Net from Wu et al. (2022). Our method trained with only 10% labeled data achieved 89.82%, 81.60%, 7.03 voxels, and 1.81 voxels for Dice, Jaccard, 95HD, and ASD. Comparing CC-Net with V-Net trained with only 10% labeled data, the Dice score improved from 78.57% to 89.82%, an improvement of 11.25%. CC-Net trained with 20% labeled data is comparable to V-Net trained with all labeled data, 91.27% vs. 91.62% for Dice, 84.02% vs. 84.60% for Jaccard, 5.75 vs. 5.40 voxels for 95HD, and 1.54 vs. 1.64 voxels for ASD. The aforementioned results demonstrated that our semi-supervised learning method effectively uses unlabeled data and can, in situations where the proportion of labeled data is low, be as effective as supervised training using fully labeled data. The two complementary auxiliary models both benefit from the complementary properties to greatly reduce the uncertainty of unlabeled data segmentation and direct the main model to produce finer and correct segmentation results. As a result, our proposed method outperforms other cutting-edge algorithms.

4.3. Qualitative analysis

Fig. 4 provides the visualization of the segmentation results for the comparison methods. As shown by the arrow in Fig. 4, the segmented uncertainty region is usually in the fine branches and local protrusions. As far as the comparison of several algorithms is concerned, DTC is more capable of segmenting branches (blue arrow in Fig. 4(d)) and can predict the basic shape of branches, but the interior of the segmentation is rougher (pink arrow in Fig. 4(d)). MC-Net+ has better overall segmentation but is easily ignored at the branches (blue arrows in Fig. 4(c)). There are more false segmentations inside the SASSNet segmentation. UA-MT has strong segmentation capability inside the segmentation but is extremely insensitive to the branches. After converting the segmentation results of each algorithm into blue point clouds and fusing them with the 3D real labels (columns 3 and 6 of Fig. 4), it is easy to see that the segmentation results of our proposed method are closer to the real labels than other advanced algorithms.

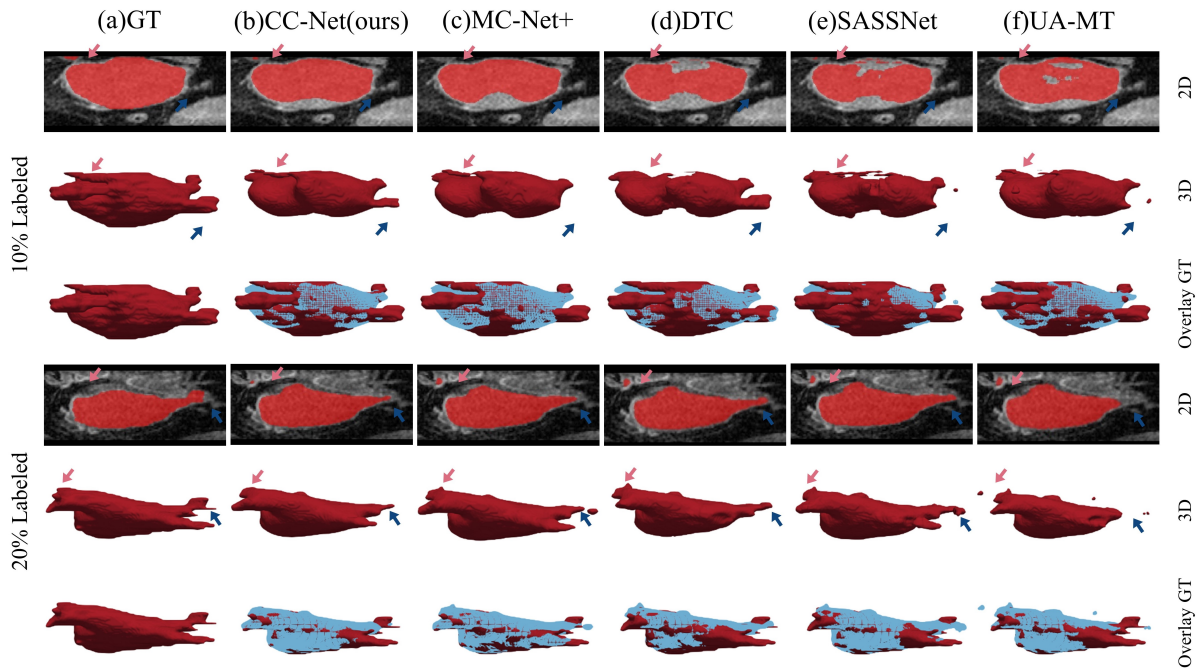
4.4. Robustness analysis

Fig. 5 shows the box plots of Dice and Jaccard for our method and other advanced methods on 20 cases of test data. The outcomes of 10% of labeled data used for training are shown in Fig. 5(a). The median of the Dice results for CC-Net is higher than MC-Net+ and DTC, and the box plot quartiles for CC-Net are smaller than those for MC-Net+ and DTC. Both the MC-Net+ and DTC box plots contain outliers. When the scatter is added, it is clear that CC-Net has a more concentrated distribution of the results of the 20 case tests and can perform better on a challenging sample.

The outcomes of 20% of labeled data used for training are shown in Fig. 5(b). The median of the Dice results for CC-Net is higher than MC-Net+ and DTC, and the box plot quartiles for CC-Net are smaller than those for MC-Net+ and DTC. The

Table 1. Comparison of quantitative results of multiple methods with 10% labeled data and 20% labeled data used for training (where data with * are from Wu et al. (2022))

Method	#Scans used		Metrics			
	Labeled	Unlabeled	Dice(%) \uparrow	Jaccard(%) \uparrow	95HD(voxel) \downarrow	ASD(voxel) \downarrow
V-Net*	8(10%)	0	78.57	66.96	21.2	6.07
V-Net*	16(20%)	0	86.96	77.31	11.85	3.22
V-Net*	80(All)	0	91.62	84.6	5.4	1.64
UA-MT (Yu et al., 2019) (MICCAI)	8(10%)	72(90%)	85.69	75.35	16.14	4.39
SASSNet (Li et al., 2020) (MICCAI)	8(10%)	72(90%)	86.8	76.9	14.57	4.11
DTC (Luo et al., 2021) (AAAI)	8(10%)	72(90%)	87.43	78.06	8.37	2.4
MC-Net (Wu et al., 2021) (MICCAI)	8(10%)	72(90%)	87.5	77.98	11.28	2.3
MC-Net+ (Wu et al., 2022) (MIA)	8(10%)	72(90%)	88.9	80.16	8.02	1.91
CC-Net(ours)	8(10%)	72(90%)	89.82	81.60	7.03	1.81
UA-MT (Yu et al., 2019) (MICCAI)	16(20%)	64(80%)	88.87	80.21	7.32	2.26
SASSNet (Li et al., 2020) (MICCAI)	16(20%)	64(80%)	89.17	80.69	8.57	2.86
DTC (Luo et al., 2021) (AAAI)	16(20%)	64(80%)	89.43	81	7.39	2.12
MC-Net (Wu et al., 2021) (MICCAI)	16(20%)	64(80%)	90.12	82.12	8.07	1.99
MC-Net+ (Wu et al., 2022) (MIA)	16(20%)	64(80%)	91.05	83.64	5.81	1.69
CC-Net(ours)	16(20%)	64(80%)	91.27	84.02	5.75	1.54

**Fig. 4. Comparison of the visual segmentation results of 10% labeled data and 20% labeled data used for training.**

lower quartile of the Dice result for CC-Net is higher than MC-Net+ and DTC, although there is one outlier in the distribution. Combined with the scatter, it is easy to see that the overall test results of CC-Net are better than MC-Net+ and DTC, and the distribution is more concentrated. The traits of the Jaccard results are essentially the same as those of the Dice results. It is clear that for the 20 test data cases, our proposed method's test results are more concentrated in terms of distribution and the overall results are better than those of the other two methods,

reflecting our method's higher level of robustness.

4.5. Ablation studies

We conduct ablation experiments from the perspective of whether or not the auxiliary model encoder is shared to confirm the validity of the proposed method architecture design in this paper. The results for the shared and standalone encoders are contrasted in Table 2. If the auxiliary model encoder is shared, it can be seen that the segmentation results are significantly

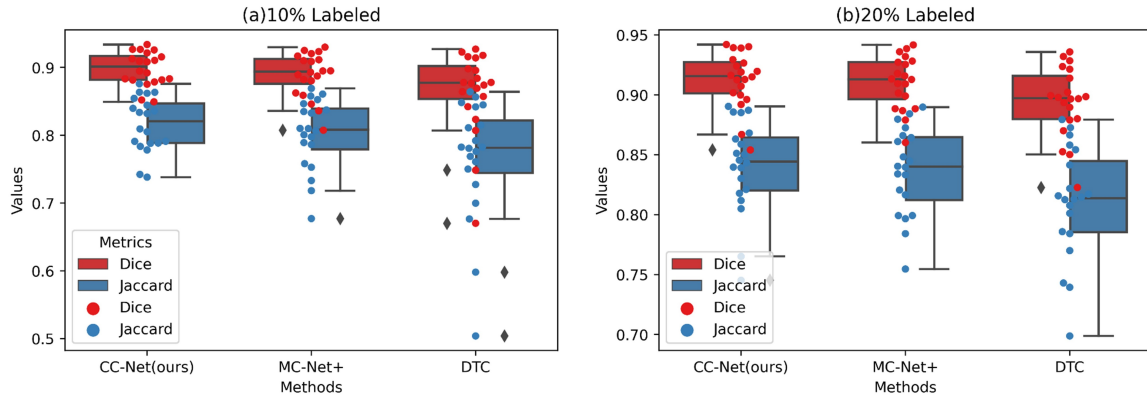


Fig. 5. Comparison of the distribution results of the 20 cases of test data.

Table 2. Performance comparison between shared and standalone encoders

Encoder	#Scans used		Metrics			
	Labeled	Unlabeled	Dice(%) \uparrow	Jaccard(%) \uparrow	95HD(voxel) \downarrow	ASD(voxel) \downarrow
Shared	8(10%)	72(90%)	84.3	73.67	16.99	4.79
Independent	8(10%)	72(90%)	89.82	81.60	7.03	1.81
Shared	16(20%)	64(80%)	87.9	78.65	9.99	2.45
Independent	16(20%)	64(80%)	91.27	84.02	5.75	1.54

worse than the standalone encoder. Although sharing encoders lessens network complexity and training time, it also unifies the encoder parameters, and even with complementary symmetric jump connections, the pseudo-labels produced by the auxiliary model do not have a part that can be learned by the main model. As a result, after sharing encoders, the auxiliary model's effectiveness is significantly reduced.

We experimentally select the best supervised loss weights λ_s . Fig. 6 provides a comparison of the test results for different λ_s . When the value of λ_s is small, the model learns less reliable information from the labeled data, resulting in poor segmentation performance. λ_s is too large, resulting in poorer consistent training, which reduces the model segmentation performance. Finally, 0.3 is chosen as the supervised loss weight in this paper.

5. Discussion

Automated left atrial segmentation algorithms based on a small amount of labeled data are important for the study and treatment of atrial fibrillation. Semi-supervised segmentation aims to improve network performance using large amounts of unlabeled data. However, current algorithms are only partially capable of extracting information from unlabeled data. In this paper, a new semi-supervised algorithm is proposed for 3D left atrial segmentation. The algorithm achieves excellent segmentation performance by effectively utilizing the unlabeled data from the perspective of complementary information.

Comparing our method to other semi-supervised algorithms is detailed in Table 1. In both settings, our approach achieves

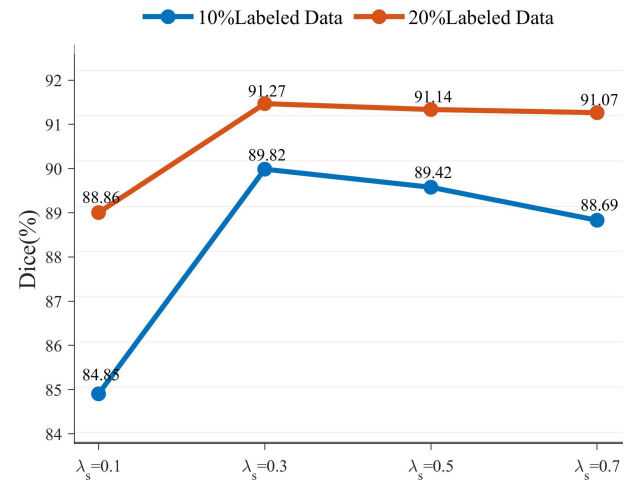


Fig. 6. Comparison of test results for different values of supervised loss weights.

the best performance. Our method achieved 91.27%, 84.02%, 5.75 voxels, and 1.54 voxels for Dice, Jaccard, 95HD, and ASD when training on 20% labeled data. Our method shows a significant improvement in segmentation performance when compared to other methods, using 10% labeled data for training. This is contributed by the complementary structure of our method, which extracts reliable information from unlabeled data. Fig. 4 provides a comparison of the 3D visualization results of different methods. It is easy to see that our method has higher confidence in the segmentation boundary in the uncertain region. As shown in Fig. 5, for the 20 cases of test data, the

results obtained by the method in this paper are more concentrated in terms of distribution and have better overall segmentation performance. This indicates that our method has stronger robustness.

Despite the good performance achieved by the method in this paper, the mining of complementary information is not sufficient. More strategies for mining complementary information will be explored in the future. The method will be applied to other medical segmentation tasks.

6. Conclusion

In this paper, a new semi-supervised learning method based on complementary consistency training is proposed for 3D left atrial image segmentation. The method makes efficient use of unlabeled data by using complementary information for consistency training. We construct two complementary auxiliary models, one focusing more on high-resolution detailed information and the other on high-level semantic information. The auxiliary models generate pseudo labels with complementary information, which in turn are trained for consistency with the main model. In the training process, on the one hand, the complementary auxiliary models are encouraged to help the main model generate high-quality segmentation results. On the other hand, the main model is encouraged to help the complementary auxiliary model generate more plausible pseudo labels. By comparing with the latest methods, CC-Net which was proposed in this paper achieves the best segmentation performance on the 2018 Atrial Segmentation Challenge dataset.

Acknowledgments

The research has been supported by the National Natural Science Foundation of China (Ref. 61903137), the Natural Science Foundation of Hunan Province (Ref. 2020JJ5201) and the Shenzhen Fundamental Research and Discipline Layout project (Ref. JCYJ20210324101215039).

References

- Chen, C., Bai, W., Rueckert, D., 2019. Multi-task learning for left atrial segmentation on ge-mri, in: Pop, M., Sermesant, M., Zhao, J., Li, S., McLeod, K., Young, A., Rhode, K., Mansi, T. (Eds.), *Statistical Atlases and Computational Models of the Heart. Atrial Segmentation and LV Quantification Challenges*, Springer International Publishing, pp. 292–301. doi:https://doi.org/10.1007/978-3-030-12029-0_32.
- Chen, J., Fu, C., Xie, H., Zheng, X., Geng, R., Sham, C.W., 2022a. Uncertainty teacher with dense focal loss for semi-supervised medical image segmentation. *Computers in Biology and Medicine* 149, 106034. URL: <https://www.sciencedirect.com/science/article/pii/S001048252200751X>, doi:<https://doi.org/10.1016/j.combiomed.2022.106034>.
- Chen, X., Yuan, Y., Zeng, G., Wang, J., 2021. Semi-supervised semantic segmentation with cross pseudo supervision, in: *Proceedings of the IEEE/CVF Conference on Computer Vision and Pattern Recognition*, pp. 2613–2622.
- Chen, X., Zhou, H.Y., Liu, F., Guo, J., Wang, L., Yu, Y., 2022b. Mass: Modality-collaborative semi-supervised segmentation by exploiting cross-modal consistency from unpaired ct and mri images. *Medical Image Analysis* 80, 102506. URL: <https://www.sciencedirect.com/science/article/pii/S1361841522001530>, doi:<https://doi.org/10.1016/j.media.2022.102506>.
- Dong-DongChen, W., WeiGao, Z.H., 2018. Tri-net for semi-supervised deep learning, in: *Proceedings of twenty-seventh international joint conference on artificial intelligence*, pp. 2014–2020.
- van Engelen, J.E., Hoos, H.H., 2020. A survey on semi-supervised learning. *Machine Learning* 109, 373–440. URL: <https://doi.org/10.1007/s10994-019-05855-6>, doi:10.1007/s10994-019-05855-6.
- Guglielmo, M., Baggiano, A., Muscogiuri, G., Fusini, L., Andreini, D., Mush-taq, S., Conte, E., Annoni, A., Formenti, A., Mancini, E.M., 2019. Multimodality imaging of left atrium in patients with atrial fibrillation. *Journal of Cardiovascular Computed Tomography* 13, 340–346. doi:<https://doi.org/10.1016/j.jcct.2019.03.005>.
- Hu, L., Li, J., Peng, X., Xiao, J., Zhan, B., Zu, C., Wu, X., Zhou, J., Wang, Y., 2022. Semi-supervised npc segmentation with uncertainty and attention guided consistency. *Knowledge-Based Systems* 239, 108021. URL: <https://www.sciencedirect.com/science/article/pii/S0950705121011205>, doi:<https://doi.org/10.1016/j.knosys.2021.108021>.
- Ikenouchi, T., Inaba, O., Takamiya, T., Inamura, Y., Sato, A., Matsumura, Y., Sato, H., Hirakawa, A., Takahashi, Y., Goya, M., Sasano, T., Nitta, J., 2021. The impact of left atrium size on selection of the pulmonary vein isolation method for atrial fibrillation: Cryoballoon or radiofrequency catheter ablation. *American Heart Journal* 231, 82–92. URL: <https://www.sciencedirect.com/science/article/pii/S0002870320303471>, doi:<https://doi.org/10.1016/j.ahj.2020.10.061>.
- Li, C., Tong, Q., Liao, X., Si, W., Sun, Y., Wang, Q., Heng, P.A., 2019. Attention based hierarchical aggregation network for 3d left atrial segmentation, in: Pop, M., Sermesant, M., Zhao, J., Li, S., McLeod, K., Young, A., Rhode, K., Mansi, T. (Eds.), *Statistical Atlases and Computational Models of the Heart. Atrial Segmentation and LV Quantification Challenges*, Springer International Publishing, pp. 255–264. doi:https://doi.org/10.1007/978-3-030-12029-0_28.
- Li, S., Zhang, C., He, X., 2020. Shape-aware semi-supervised 3d semantic segmentation for medical images, in: *International Conference on Medical Image Computing and Computer-Assisted Intervention*, Springer, pp. 552–561. doi:https://doi.org/10.1007/978-3-030-59710-8_54.
- Liu, Y., Wang, W., Luo, G., Wang, K., Li, S., 2022. A contrastive consistency semi-supervised left atrium segmentation model. *Computerized Medical Imaging and Graphics* 99, 102092. doi:<https://doi.org/10.1016/j.compmedimag.2022.102092>.
- Luo, X., Chen, J., Song, T., Wang, G., 2021. Semi-supervised medical image segmentation through dual-task consistency, in: *Proceedings of the AAAI Conference on Artificial Intelligence*, pp. 8801–8809. doi:<https://doi.org/10.1609/aaai.v35i10.17066>.
- Milletari, F., Navab, N., Ahmadi, S.A., 2016. V-net: Fully convolutional neural networks for volumetric medical image segmentation, in: *2016 Fourth International Conference on 3D Vision (3DV)*, pp. 565–571. doi:10.1109/3DV.2016.79.
- Ouali, Y., Hudelot, C., Tami, M., 2020. Semi-supervised semantic segmentation with cross-consistency training, in: *Proceedings of the IEEE/CVF Conference on Computer Vision and Pattern Recognition*, pp. 12674–12684.
- Wang, J., Liu, X., Yin, J., Ding, P., 2022a. Dc-net: Dual-consistency semi-supervised learning for 3d left atrium segmentation from mri. *Biomedical Signal Processing and Control* 78, 103870. URL: <https://www.sciencedirect.com/science/article/pii/S1746809422003858>, doi:<https://doi.org/10.1016/j.bspc.2022.103870>.
- Wang, K., Zhan, B., Zu, C., Wu, X., Zhou, J., Zhou, L., Wang, Y., 2022b. Semi-supervised medical image segmentation via a tripled-uncertainty guided mean teacher model with contrastive learning. *Medical Image Analysis* 79, 102447. doi:<https://doi.org/10.1016/j.media.2022.102447>.
- Wu, Y., Ge, Z., Zhang, D., Xu, M., Zhang, L., Xia, Y., Cai, J., 2022. Mutual consistency learning for semi-supervised medical image segmentation. *Medical Image Analysis* 81, 102530. doi:<https://doi.org/10.1016/j.media.2022.102530>.
- Wu, Y., Xu, M., Ge, Z., Cai, J., Zhang, L., 2021. Semi-supervised left atrium segmentation with mutual consistency training, in: *International Conference on Medical Image Computing and Computer-Assisted Intervention*, Springer, pp. 297–306. doi:https://doi.org/10.1007/978-3-030-87196-3_28.
- Xia, Y., Yang, D., Yu, Z., Liu, F., Cai, J., Yu, L., Zhu, Z., Xu, D., Yuille, A., Roth, H., 2020. Uncertainty-aware multi-view co-training for semi-supervised medical image segmentation and domain adaptation. *Medical*

- Image Analysis 65, 101766. URL: <https://www.sciencedirect.com/science/article/pii/S1361841520301304>, doi:<https://doi.org/10.1016/j.media.2020.101766>.
- Xiao, Z., Su, Y., Deng, Z., Zhang, W., 2022. Efficient combination of cnn and transformer for dual-teacher uncertainty-guided semi-supervised medical image segmentation. *Computer Methods and Programs in Biomedicine* 226, 107099. URL: <https://www.sciencedirect.com/science/article/pii/S0169260722004801>, doi:<https://doi.org/10.1016/j.cmpb.2022.107099>.
- Xiong, Z., Xia, Q., Hu, Z., Huang, N., Bian, C., Zheng, Y., Vesal, S., Ravikumar, N., Maier, A., Yang, X., 2021. A global benchmark of algorithms for segmenting the left atrium from late gadolinium-enhanced cardiac magnetic resonance imaging. *Medical Image Analysis* 67, 101832. doi:<https://doi.org/10.1016/j.media.2020.101832>.
- Yan, X., Hu, S., Mao, Y., Ye, Y., Yu, H., 2021. Deep multi-view learning methods: a review. *Neurocomputing* 448, 106–129. doi:<https://doi.org/10.1016/j.neucom.2021.03.090>.
- Yu, L., Wang, S., Li, X., Fu, C.W., Heng, P.A., 2019. Uncertainty-aware self-ensembling model for semi-supervised 3d left atrium segmentation, in: *International Conference on Medical Image Computing and Computer-Assisted Intervention*, Springer. pp. 605–613. doi:https://doi.org/10.1007/978-3-030-32245-8_67.
- Zhai, D., Hu, B., Gong, X., Zou, H., Luo, J., 2022. Ass-gan: Asymmetric semi-supervised gan for breast ultrasound image segmentation. *Neurocomputing* 493, 204–216. URL: <https://www.sciencedirect.com/science/article/pii/S0925231222003885>, doi:<https://doi.org/10.1016/j.neucom.2022.04.021>.
- Zhang, Z., Tian, C., Bai, H.X., Jiao, Z., Tian, X., 2022. Discriminative error prediction network for semi-supervised colon gland segmentation. *Medical Image Analysis* 79, 102458. URL: <https://www.sciencedirect.com/science/article/pii/S1361841522001050>, doi:<https://doi.org/10.1016/j.media.2022.102458>.
- Zheng, X., Fu, C., Xie, H., Chen, J., Wang, X., Sham, C.W., 2022. Uncertainty-aware deep co-training for semi-supervised medical image segmentation. *Computers in Biology and Medicine* , 106051doi:<https://doi.org/10.1016/j.compbiomed.2022.106051>.
- Zhong, Y., Yuan, B., Wu, H., Yuan, Z., Peng, J., Wang, Y.X., 2021. Pixel contrastive-consistent semi-supervised semantic segmentation, in: *Proceedings of the IEEE/CVF International Conference on Computer Vision*, pp. 7273–7282.